Journal of Materials Chemistry C

Accepted Manuscript

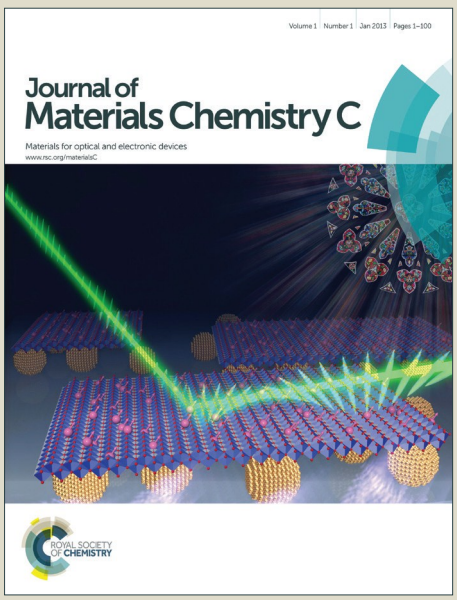

ROYAL SOCIETY OF CHEMISTRY

www.rsc.org/materialsC

ARTICLE Journal of Materials Chemistry C

$Ba_6(Bi_{1-x}Eu_x)_9B_{79}O_{138}$ ($0 \le x \le 1$): synergetic changing of the wavelength of Bi^{3+} absorption and the red-to-orange emission ratio of Eu^{3+}

Cite this: DOI: 10.1039/xoxx00000x

Received ooth January 2012,
Accepted ooth January 2012

DOI: 10.1039/xoxx00000x

www.rsc.org/

Qiaoqi Li,[a] Rihong Cong,[a*] Xianju Zhou,[b] Wenliang Gao,[a] and Tao Yang[a*]

Very recently, a novel barium bismuth borate $Ba_6Bi_9B_{79}O_{138}$ (**BBBO**) was proved to be a new analogue of $RE BaB_9O_{16}$ (*RE* = rare earth), which is a big family of excellent phosphor hosts, because there are two types of cationic positions suitable for bi- and tri-valent activators (or sensitizers), respectively. In this study, we prepared Eu^{3+}-to-Bi^{3+} substituted solid solutions $Ba_6(Bi_{1-x}Eu_x)_9B_{79}O_{138}$ ($0 \le x \le 1$) and performed a systematic UV-photoluminescence investigation. As anticipated, the efficient energy transfer occurs in the whole series of compounds, and the majority energy absorbed by Bi^{3+} was transmitted to Eu^{3+}, causing an great enhancement of Eu^{3+} emission. More interestingly, the Eu^{3+}-to-Bi^{3+} substitution leads to a centrosymmetric-to-noncentrosymmetric transition of the local coordination symmetry of trivalent cations, due to the size difference between Eu^{3+} and Bi^{3+}. It presents as the synergetic changing in the wavelength of Bi^{3+} $^1S_0 \rightarrow {}^3P_1$ absorption (in the excitation spectra) and the red-to-orange emission ratio (in emission spectra) when changing *x*. **BBBO** is a new polyborate host with a freshly resolved structure, the preliminary and interesting results promote us to further develop **BBBO**-based phosphors.

Introduction

Borates are well known good hosts for luminescent materials due to their high transparency, excellent chemical and thermal stability, and high luminescence efficiency.[1-3] The major structural characteristic is the rigid covalent boron-oxygen network. Among them, polyborates with $B/M \ge 3$ (*M* = metal) are especially attractive because the luminescent activators can be spatially separated by large polyborate anions and thus the concentration quenching can be postponed or even eliminated.[4,5] For example, the absence of concentration quenching was reported in Eu^{3+}- and Tb^{3+}-doped α-GdB_5O_9 phosphors.[6,7]

$REMB_9O_{16}$ (*RE*= rare earth, *M* = Sr or Ba) is a series of well-known phosphor hosts with the advantage of containing two types of cations, RE^{3+} and M^{2+}.[8-10] Therefore, people can obtain highly efficient blue, green, and red phosphors by doping different activators, such as Eu^{2+}, Mn^{2+} and Eu^{3+}, Tb^{3+}.[10-12] Massive efforts have been devoted to investigate their photoluminescent (PL) properties, such as $REMB_9O_{16}$:Tb^{3+}, Ce^{3+} (*RE* = La, Gd, and Y, *M* = Sr or Ba),[9] $RE BaB_9O_{16}$:Eu^{3+} (*RE* = La, Gd, and Y),[10,11,13,14] $GdBaB_9O_{16}$:*RE* (*RE* = Gd, Sm, Dy, Pr, Nd),[15-18] $LaBaB_9O_{16}$:*M* (*M* = Bi^{3+}, Mn^{2+}),[12] and $EuBaB_9O_{16}$.[19,20] These materials potentially have applications in white light-emitting diodes (WLED),[20] tricolour lamps,[11,21] plasma display panels (PLD) under VUV excitation,[13,22] and as well as laser materials.[23] However, in contrast to the extensive studies on PL properties, the knowledge on the crystal structure of $REMB_9O_{16}$ was very limited.[9-11,23,24]

Very recently, a novel barium bismuth borate $Ba_6Bi_9B_{79}O_{138}$ (**BBBO**) was proved to be a new analogue of $REMB_9O_{16}$.[25] Single crystal X-ray diffraction (XRD) characterizations proposed an ordered structure model in the noncentrosymmetric space group *R*3 with the parameters a = 7.841(1) Å and c = 46.557(9) Å.[25] It possesses a layered-type structure constructed by the alternating stacking of BO_4-BiO_6-BO_4 and polyborate layers. Ba^{2+} atoms locate in the inter-layer cavities, which are ten-coordinated. There are three and two crystallographically independent Bi^{3+} and Ba^{2+}, respectively.[25]

Based on the outstanding PL performance of $REMB_9O_{16}$,[9-20] we believe the presence of Bi^{3+} in this particular host matrix (**BBBO**) could provide an additional positive factor and interesting variety on the PL study because Bi^{3+} is a commonly used sensitizer.[26,27] In this report, the UV-excited PL properties of $Ba_6(Bi_{1-x}Eu_x)_9B_{79}O_{138}$ (**BBBO:*x*Eu^{3+}**, $0 \le x \le 1$) were systematically investigated. Indeed, an efficient energy transfer from Bi^{3+} to Eu^{3+} was observed, leading to bright and pure-red phosphors.

It is well known that the luminescence of Eu^{3+} is a good medium to gain structural information about the short-range and local coordination environment of Eu^{3+} cations.[6,11] Here, it is very interesting to observe the simultaneous evolution in the wavelength shifting of Bi^{3+} $^1S_0 \rightarrow {}^3P_1$ absorption (in the excitation spectra) and the changing of red-to-orange emission ratio (in emission spectra) when changing x in $Ba_6(Bi_{1-x}Eu_x)_9B_{79}O_{138}$. For instance, there are three regions, x = 0.01-0.30; 0.30-0.70, and 0.70-1. Eu^{3+}/Bi^{3+} cations locate at a close-to-centrosymmetric coordination environment in **BBBO** host in the first region; by doping an appropriate concentration of Eu^{3+} into **BBBO**, the local coordination symmetry of Eu^{3+}/Bi^{3+} deviates from the inversion center, which starts at about x = 0.30 and finishes at about x = 0.70; when x > 0.70, the local coordination of Eu^{3+}/Bi^{3+} is far away from centrosymmetric and almost unchanged.

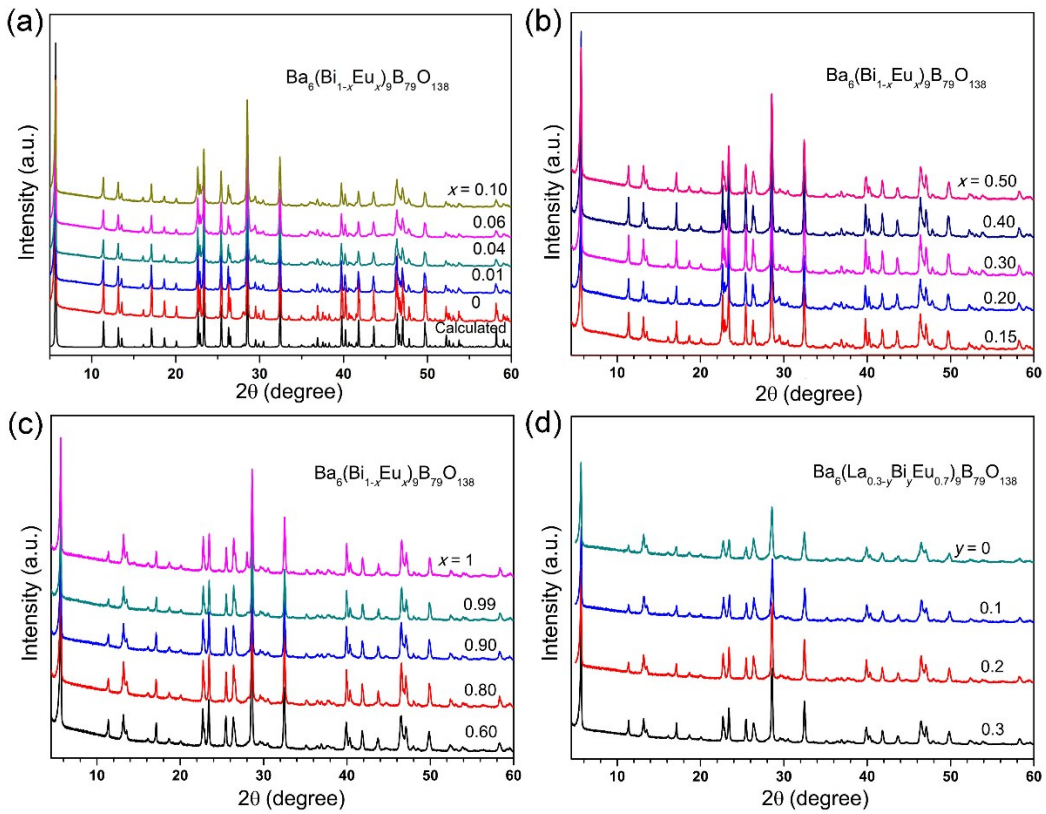

Fig. 1 X-ray diffraction patterns for **BBBO:*x*Eu^{3+}** ($0 \le x \le 1$) and $Ba_6(La_{0.3-y}Bi_yEu_{0.7})_9B_{79}O_{138}$ ($(0 \le y \le 0.3)$. A calculated XRD pattern from the single crystal structure of **BBBO** was given for comparison.

Experimental

Synthesis

All samples in this series were synthesized by high temperature solid state reactions. The starting materials, H_3BO_3 and Bi_2O_3, were of analytical grade and used as obtained from commercial sources without further purification; $BaCO_3$, Eu_2O_3 and La_2O_3, were of high purity and used after a pre-calcination at 800 ℃ to remove the possible absorbed water or CO_2 from air. Typically, for the synthesis of **BBBO:*x*Eu^{3+}**, stoichiometric mixtures of $BaCO_3$, Bi_2O_3, Eu_2O_3, and H_3BO_3 (excess of about 10 at% to compensate for the volatilization of boron oxide at high temperature) were ground in an agate mortar adequately and pressed into small pellets, which were pre-heated slowly (0.5 ℃/min) up to 550 ℃ and kept for 15 hours to decompose the carbonate and boric acid. Care was taken to avoid any partial melting of the samples. After extensive re-grinding, the mixtures were pressed into small pellets again and sintered at 650 ℃ for 15 hours. With an intermediate grinding, the mixtures were then heated for another 15 hours at the final reaction temperatures, which varied from 700 to 830 ℃ along with the increase of Eu^{3+} content. $Ba_6(La_{0.3-y}Bi_yEu_{0.7})_9B_{79}O_{138}$ was synthesized with a similar procedure, and the final reaction temperature was 850 ℃.

Characterizations

Powder XRD data were collected at room temperature using a PANalytical X'pert diffractometer equipped with a PIXcel 1D detector (Cu Kα, 40 kV and 40 mA). Le Bail refinements were performed to obtain the cell parameters using TOPAS software package.[28] During the refinements, the first diffraction peak (at about 5.6 °/2θ) was excluded because this peak usually has a largely asymmetric shape and different with others. General photoluminescence spectra were measured on a Hitachi F4600 fluorescence spectrometer at room temperature. The voltage of the Xe lamp was fixed to be 700 V, and both of the input and output slits were selected to be 1.0 nm. The emission intensities were calculated from the integral of the corresponding peaks. The emission spectrum at low temperature was recorded by an Edinburgh FLS-920 spectrophotometer equipped with a 450 W xenon lamp and a pulse xenon lamp as light sources. The powder sample was placed in a helium gas flow cryostat for getting a low temperature as 10 K. Quantum yields (QY) were measured with an integrating sphere in the same instrument at room temperature. Photographs of phosphors under a 254 nm UV lamp excitation were taken by a digital camera.

Results and Discussion

Phase purity analysis

Powder XRD patterns of **BBBO:*x*Eu^{3+}** and $Ba_6(La_{0.3-y}Bi_yEu_{0.7})_9B_{79}O_{138}$ are shown in Fig. 1, where all patterns share the same characteristic with **BBBO**,[25] showing no impurity peak. It is not surprise about the readily formation of these solid solutions because of the very close cationic radii of Bi^{3+} (1.03 Å for six-coordinated), Eu^{3+} (0.947 Å) and La^{3+} (1.032 Å). As shown in Figs. 1a-1c, the diffraction peaks show a slight right-shift to higher angles with the increase of Eu^{3+} content in **BBBO:*x*Eu^{3+}**, which has been reported in literature,[25] indicating a linear shrinkage of the unit cell volume (from 2485.6 to 2453.9 Å^3). As shown in Fig. 1d, the unit cell change of $Ba_6(La_{0.3-y}Bi_yEu_{0.7})_9B_{79}O_{138}$ caused by Bi^{3+}-to-La^{3+} doping is not that obvious because of the almost same cationic radii of La^{3+} and Bi^{3+}. Nevertheless, we could monitor the change of the cell lattice parameters (*a*, *c* and *V*) by Le Bail fitting on the powder XRD patterns (see Table S1 in the ESI). The variation of the cell volume from 2466.9 to 2463.5 Å^3 suggests a gentle shrinkage when *y* increases from 0 to 0.3 (See Fig. S1). All the above observations ensure the successful cationic substitution, after which a systematic study on structural-photoluminescence relationship of **BBBO:*x*Eu^{3+}** and $Ba_6(La_{0.3-y}Bi_yEu_{0.7})_9B_{79}O_{138}$ is valid to proceed.

Photoluminescence of BBBO host

Bi^{3+} is a commonly used sensitizer in PL research, and it is an activator as well.[26,27,29] Therefore we need to take a look at the luminescence behavior of the host **BBBO** without any dopant before the study on the **BBBO:*x*Eu^{3+}** phosphors. Bi^{3+} possesses $6s^2$ lone pair electrons, therefore the position of its excitation and emission bands depends largely on the nature of the host lattice.[27] As shown in Fig. 2, there is a broad excitation band centering at 275 nm and a broad emission band ranging from 300 to 600 nm with the maximum at 398 nm.

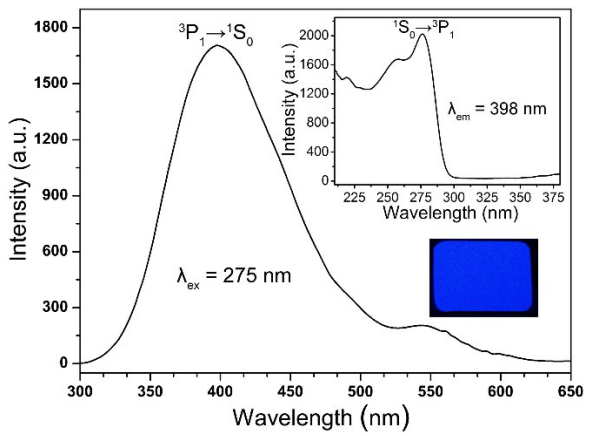

Fig. 2 Emission and excitation spectra of **BBBO** without any dopant at room temperature (λ_{ex} = 275 nm, λ_{em} = 398 nm, respectively). The bottom-right insert shows the digital photograph of **BBBO** powder under a 254 nm UV lamp irradiation. Due to the relative weak intensity of these spectra comparing with other Eu^{3+} doped samples, the input and output slits during the PL measurements were selected to be 2.5 nm.

Bi^{3+} has a ground state $^1S_0$ and the corresponding excited states are $^3P_0$, $^3P_1$, $^3P_2$ and $^1P_1$. For the electron transition of the Bi^{3+} ions, $^1S_0 \rightarrow {}^1P_1$ is allowed for $\Delta S = 0$ according to the spin-selection rule, which is usually located below 200 nm. While the $^1S_0 \rightarrow {}^3P_0$ transition is strongly forbidden because total angular momentum is not changed ($\Delta J = 0$). $^1S_0 \rightarrow {}^3P_1$ is usually forbidden for spin-selection rule, it can be partially allowed by mixing singlet and triplet states ($\Delta J = 1$).[27,30,31] Therefore, we interpret the broad excitation band observed in Fig. 2 to be $^1S_0 \rightarrow {}^3P_1$ absorption of Bi^{3+}. The wide emission band at 398 nm was attributed to $^3P_1 \rightarrow {}^1S_0$ transition of Bi^{3+} according to the literature.[27] Moreover, a beautiful blue emission can be observed by naked eyes under a 254 nm UV lamp irradiation as shown in Fig. 2.

Excitation spectra in BBBO:*x*Eu^{3+} ($0 \le x \le 1$)

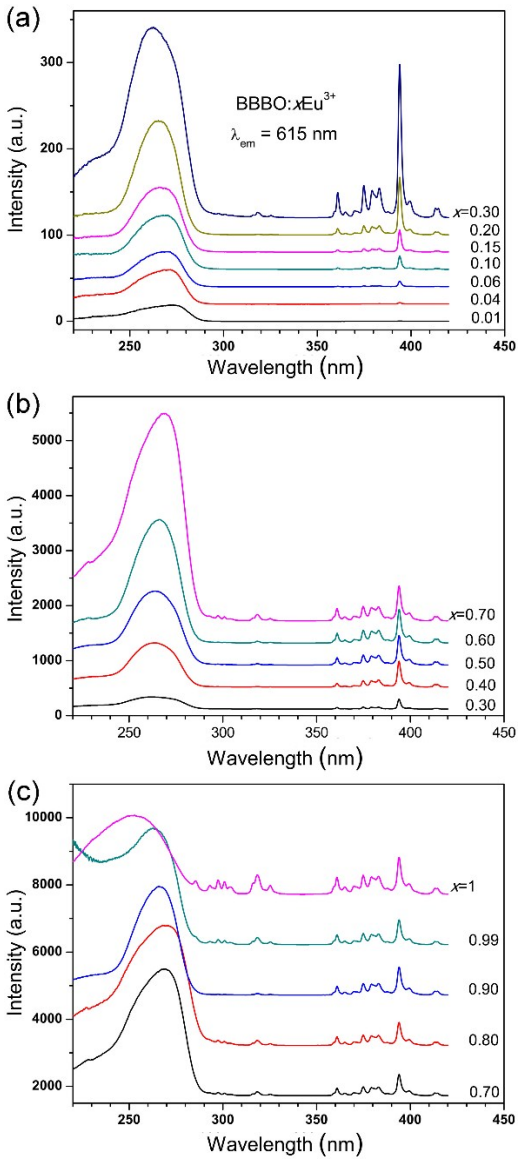

Fig. 3 Excitation spectra of **BBBO:*x*Eu^{3+}** ($0 \le x \le 1$) samples (λ_{em} = 615 nm). For better presentation and comparison, the spectra were shifted along the y-axis.

Fig. 3 shows the excitation spectra of **BBBO:*x*Eu^{3+}** by monitoring the Eu^{3+} emission at 615 nm. The excitation spectra

consist of the intense broad bands in the shorter wavelength region, and some sharp peaks in the longer wavelength region when $x \geq 0.04$. It is clear that these sharp peaks in the region from 290 to 420 nm are due to the $4f^6 \rightarrow 4f^6$ transitions of Eu^{3+} ions, whose positions are almost unchanged along with the increasing x due to their inert nature to the host lattice.[6,11] However, the position of the broad band shows a difference, especially for that of the sample with $x = 1$ (named as **BEBO**) as shown in Fig. 3c. Obviously, the broad band centering at 252 nm in the excitation spectrum of **BEBO** is the typical absorption of $O^{2-} \rightarrow Eu^{3+}$charge transfer (CT),[6,11] and the wide bands for other samples can be readily contributed to the $^1S_0 \rightarrow {}^3P_1$ transition of Bi^{3+} by referring to the excitation spectrum of **BBBO** host (see Fig. 2). The $O^{2-} \rightarrow Eu^{3+}$ CT transition is not observed when $x = 0.01$-0.90 due to the relative weak intensity and possible overlapping with the absorption of Bi^{3+}. The main point is that the presence of the strong Bi^{3+} absorption in the excitation spectra by monitoring Eu^{3+} emission indicates an energy transfer from Bi^{3+} to Eu^{3+}. Moreover, the presence of such an efficient energy transfer proves that the doping ion of Eu^{3+} occupies the position of Bi^{3+} rather than Ba^{2+} in **BBBO**, because the distances of the positions of Bi^{3+} and Ba^{2+} are too long for energy transfer.[25]

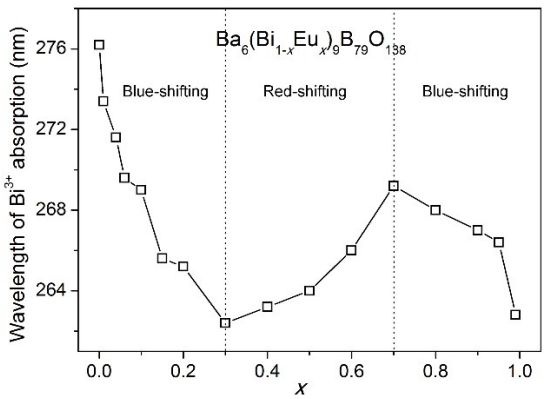

Fig. 4 The excitation wavelength of Bi^{3+} $^1S_0 \rightarrow {}^3P_1$ absorption band in **BBBO:*x*Eu^{3+}** ($0 \leq x \leq 1$) as a function of Eu^{3+} content (x).

As shown in Fig. 3, the intensity of the *f-f* absorption of Eu^{3+} increases gradually along with x. While the intensity of the absorption band of Bi^{3+} increases until $x = 0.70$, and decreases slightly in the higher Eu^{3+} concentrations. Moreover, on contrast to the inert nature of $4f^6 \rightarrow 4f^6$ transition, an obvious shift of wavelength was observed for the $^1S_0 \rightarrow {}^3P_1$ absorption of Bi^{3+} along with x as shown in Fig. 3. It becomes quite interesting when plotting such a variation as a function of x (see Fig. 4), which can be divided into three regions. For example, the excitation of Bi^{3+} shifts towards a shorter wavelength by increasing the Eu^{3+} content when $x < 0.30$; it reaches a minimum at $x = 0.30$, and a red-shifting occurs until $x = 0.70$; when $x > 0.70$, there was a blue-shifting once again. Such a variation on the position for Bi^{3+} absorption, i.e. two turning points along with the increase of x, suggests a complicated evolution of the local coordination environment of Bi^{3+}/Eu^{3+}, which is indeed interesting and will be discussed in later sections.

Emission spectra of BBBO:*x*Eu^{3+} ($0 \leq x \leq 1$)

The compositional dependence of emission spectra under the excitation of $^1S_0 \rightarrow {}^3P_1$ absorption band of Bi^{3+}were given in Fig. 5, except that the excitation for **BEBO** is the $O^{2-} \rightarrow Eu^{3+}$ CT transition. The emission spectra of above compounds are all typical for Eu^{3+}, but show different characteristics. Looking at the region with the wavelength from 560 to 720 nm, four groups of emission peaks at about 585-600, 600-630, 650-665, and 690-710 nm are predominant, which are readily attributed to the typical $^5D_0 \rightarrow {}^7F_J$ (J = 1-4) transitions of Eu^{3+} ion, respectively.[11]

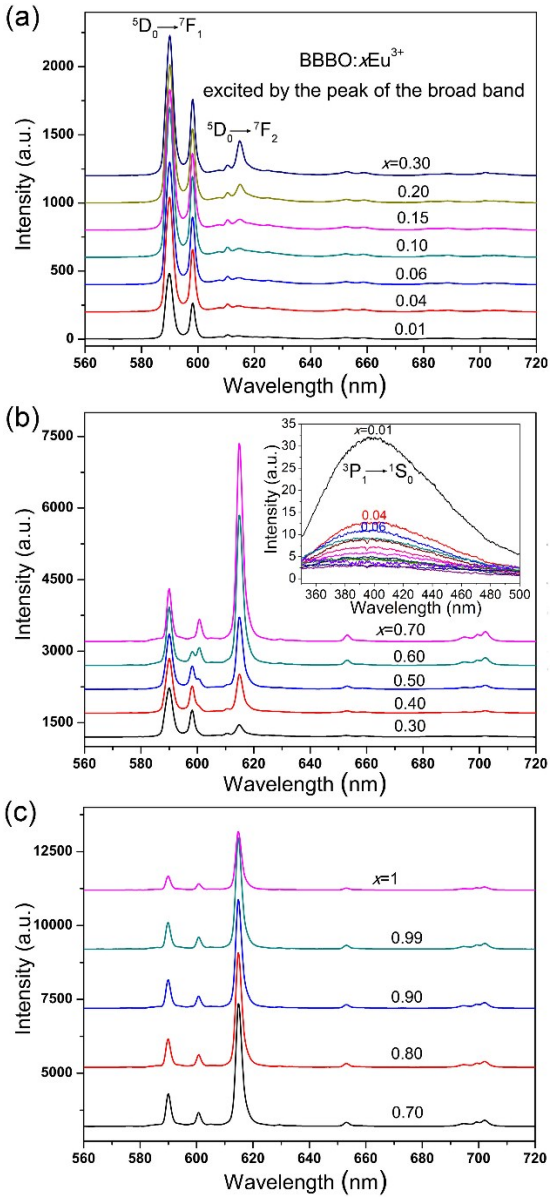

Fig. 5 Emission spectra of **BBBO:*x*Eu^{3+}** ($0 \leq x \leq 1$) excited by Bi^{3+} $^1S_0 \rightarrow {}^3P_1$ absorption. The only exception is that t the excitation for **BEBO** is the $O^{2-} \rightarrow Eu^{3+}$ CT transition. The insert presents the emission spectra measured in the region of 350-500 nm.

The non-degenerate $^5D_0 \rightarrow {}^7F_0$ emission lines are particularly important for revealing the numbers of crystallographically nonequivalent sites in a given host matrix. However, the

$^5D_0 \rightarrow {}^7F_0$ transitions in **BBBO:*x*Eu^{3+}** at 575-581 nm are very weak at room temperature and are only detectable when $x \geq 0.60$. Hence, we measured the emission spectrum at 10 K for **BBBO:0.20Eu^{3+}** (under 269 nm excitation), where two sharp peaks were observed at 576.2 and 578.1 nm respectively (see Fig. 6), indicating that the doped Eu^{3+} cations went into at least two different Bi^{3+} sites in **BBBO** host when $x = 0.20$. In literature, three $^7F_0 \rightarrow {}^5D_0$ excitation peaks were observed for $BaEuB_9O_{16}$ in a site-selective laser excitation spectrum, which means there are three different crystallographic sites for Eu^{3+}.[19] By closely looking at the Bi-O octahedra in **BBBO** (see Fig. S2 in ESI),[25] Bi1 and Bi2 have very similar coordination, which is slightly different with that of Bi3. Accordingly, we could speculate that the two-peak characteristic for **BBBO:0.20Eu^{3+}** could be due to the energy overlapping of $^5D_0 \rightarrow {}^7F_0$ transitions.

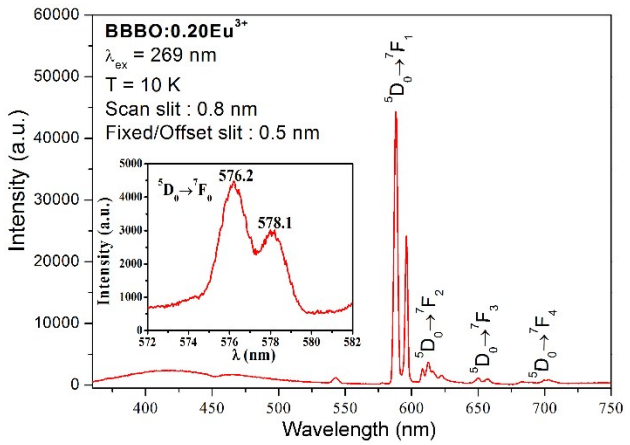

Fig. 6 Low temperature emission spectrum for **BBBO:0.20Eu^{3+}** excited by 269 nm. The insert shows the $^5D_0 \rightarrow {}^7F_0$ transitions, which are assigned at 576.2 and 578.1 nm, respectively.

In fact, the emission spectra of **BBBO:*x*Eu^{3+}** were also investigated from 350 nm to 500 nm in order to further confirm the efficiency of energy transfer. The intensities in this region of 350-500 nm are very weak as shown in the insert in Fig. 5b. The aboard band can be readily assigned to the $^3P_1 \rightarrow {}^1S_0$ transition of Bi^{3+}, which decreases rapidly when x increases. The very small residual emission of Bi^{3+} in **BBBO:*x*Eu^{3+}** samples points out the majority of the absorbed energy of Bi^{3+} transfers to Eu^{3+}.

As shown in Fig. 5, $^5D_0 \rightarrow {}^7F_1$ transitions present as the strongest peaks when $x < 0.5$, while the strongest peaks turn to be $^5D_0 \rightarrow {}^7F_2$ emissions when $x \geq 0.50$. It is known that the electric dipole-dipole transition ($^5D_0 \rightarrow {}^7F_2$) of Eu^{3+} is a symmetry-sensitive transition, which appears dominantly only when the position of Eu^{3+} deviates from the inversion center; while the magnetic dipole transition ($^5D_0 \rightarrow {}^7F_1$) is not that affected by the surrounding environment of Eu^{3+}.[11] Therefore, the different emission characteristics of **BBBO:*x*Eu^{3+}** as shown in Fig. 5 implies the local structure around Eu^{3+} changes along with the increase of x.

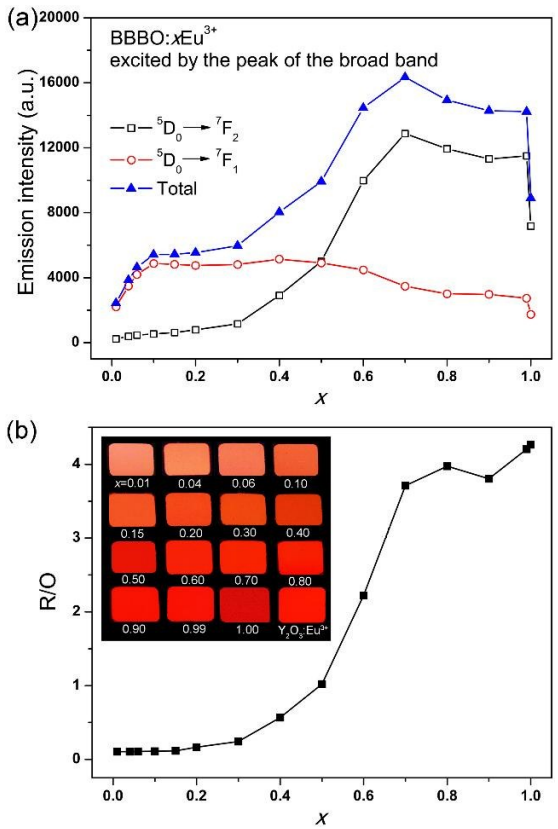

Fig. 7 (a) Dependence of the emission intensities of **BBBO:*x*Eu^{3+}** ($0 \leq x \leq 1$) excited by Bi^{3+} $^1S_0 \rightarrow {}^3P_1$ absorption; (b) R/O values against the doping concentration x. The insert shows the digital photographs of **BBBO:*x*Eu^{3+}** powder under a 254 nm UV lamp excitation.

In particular, the calculated emission intensities of $^5D_0 \rightarrow {}^7F_1$, $^5D_0 \rightarrow {}^7F_2$ and the total emission intensity were all presented in Fig. 7a along with Eu^{3+} content (x). The intensity of $^5D_0 \rightarrow {}^7F_2$ transitions first increases slowly when $x \leq 0.30$. It increases sharply when $0.30 \leq x \leq 0.70$, and then decreases slightly at higher Eu^{3+} concentrations. On the other hand, the intensity of $^5D_0 \rightarrow {}^7F_1$ transition increases gradually as x increase from 0.01 to 0.10, and keeps almost unchanged in the range of $0.10 \leq x \leq 0.40$; after that, it decreases slightly. It is well known that the intensity ratio of R/O = $I(^5D_0 \rightarrow {}^7F_2)/I(^5D_0 \rightarrow {}^7F_1)$ is recognized as a probe of the site symmetry for Eu^{3+}. Generally, a lower symmetry of the crystal field around Eu^{3+} leads to a larger R/O. Fig. 7b gives the variation of the calculated R/O values along with x, which can be divided into three regions, x = 0.01-0.30; 0.30-0.70, and 0.70-1. Keep in mind that it is consistent with the three-region-characteristics of the Bi^{3+} absorption bands changing along with x.

In the first region, the values of R/O are lower than 0.24. The small values indicate the surrounding environment of Eu^{3+} in **BBBO** is likely centrosymmetric. This result agrees with the reported crystal structure of **BBBO**, in which the Bi^{3+} ions are all coordinated by six oxygen atoms in regular octahedra, thus the ligand field around Bi^{3+} are close to centrosymmetric (see Fig. S2 in ESI).[25] In the second region with $0.30 \leq x \leq 0.70$, a further substitution of Eu^{3+} results in a rapid increase of R/O from 0.24

to 3.71, indicating the symmetry of the surrounding environment of Eu^{3+} changes from close-to-centrosymmetric to noncentrosymmetric gradually. And then, the change becomes minor in the third region. According to the above observations, we can conclude that (i) the Bi^{3+} ions are located at a centrosymmetric coordination environment in **BBBO** host; (ii) by doping an appropriate concentration of Eu^{3+} ion in **BBBO**, the symmetry of the local coordination of Eu^{3+} deviates from the inversion center, which starts at about $x = 0.30$ and finishes at about $x = 0.70$; (iii) when $x > 0.70$, the local coordination of Eu^{3+} is far away from centrosymmetric and almost unchanged.

Site symmetry evolution of Bi^{3+}/Eu^{3+} in BBBO:xEu^{3+} ($0 \le x \le 1$)

Similar speculations on symmetry evolution of the Eu^{3+} coordination have been performed by Lin et. al. during the luminescence study of LnBaB$_9$O$_{16}$:Eu^{3+} (Ln = La, Gd, Y and Lu), which revealed that the local symmetry of the rare earth ions is centrosymmetric if Ln = Y or Lu and noncentrosymmetric when Ln = La or Gd.[4,11] Moreover, similar centrosymmetric-to-noncentrosymmetric change on site symmetry was observed in $Y_{1-x}Gd_xBaB_9O_{16}$:Eu^{3+}, which occurs in the region with $0.10 \le x \le 0.60$.[11] It is clear that the local structure around rare-earth ions in this series of phosphors changes gradually according to the ionic radii of the rare-earth cations, and the critical cationic size is roughly in-between Y^{3+} and Gd^{3+}.[11]

Here, the PL study indicates that the introduction of Eu^{3+} into **BBBO** host lattice unambiguously induces a significant change of the local symmetry around Eu^{3+}/Bi^{3+}. However, it is almost impossible to monitor the Bi/Eu-O bond-distance changing by powder X-ray diffraction technique because of the very complex structure and the thus the large number of the variables of structural parameters. It might work by employing single crystal XRD, while the single crystal growth of the whole series of compounds is not in the scope of current work. It is believed that the PL spectra of Eu^{3+} are highly sensitive to the local coordination and thus the best medium to gain more local structural information of rare earth cations when doping Eu^{3+} into **BBBO**.

As discussed above, the intensity variations as shown in Fig. 7a are complicated, which are mainly due to the symmetry change along with x. For example, when $x < 0.30$, the coordination of Eu^{3+} keeps as close-to-centrosymmetric, so $^5D_0 \rightarrow {}^7F_1$ is the major emission, whose intensity increases along with x, and reaches a maximum at $x = 0.10$. In the meantime, the emission of $^5D_0 \rightarrow {}^7F_2$ transition is enhanced slowly originated from the increase concentration of the activator centers (Eu^{3+}). When $x \ge 0.30$, the growing of the intensity of $^5D_0 \rightarrow {}^7F_2$ becomes very fast, while a slight decline was found for $^5D_0 \rightarrow {}^7F_1$ emissions. Such a change is correlated with the symmetry change from centrosymmetric to noncentrosymmetric of the local structure of Eu^{3+} in the region of $0.30 \le x \le 0.70$. With further increasing $x > 0.70$, a slight emission quenching was observed.

It should be noted that no concentration quenching was observed for LnBaB$_9$O$_{16}$ (Ln = La, Gd, Y, Lu) in literature,[4] because the well separation of the activators. Therefore we speculate the slight intensity decrease in **BBBO:xEu^{3+}** from x = 0.70 to 0.99 is due to the concentration decrease of sensitizer Bi^{3+}. Moreover, the last sudden drop of the emissions from **BBBO:0.99Eu^{3+}** to **BEBO** is due to the absent of the energy transfer effect from Bi^{3+} to Eu^{3+}. In other words, both symmetry changing and energy transfer dominate the PL performance of **BBBO:xEu^{3+}**.

Highly efficient colour-tunable red-emitting phosphors can be obtained, as shown in the insert in Fig. 7b. **BBBO:xEu^{3+}** samples show tunable luminescence from orange to pure red, and the brightness and colour purity of **BBBO:0.70Eu^{3+}** are comparable with the commercial red phosphor Y_2O_3:Eu^{3+}. QY is an important parameter for phosphors. Table 1 summarizes the quantum yields of some selected phosphors. High QY values for **BBBO:xEu^{3+}** were observed under 269 nm excitation, which show a maximum of 86% when $x = 0.70$. As a comparison, the QY of commercial Y_2O_3:Eu^{3+} was also measured under a 254 nm excitation, which is close to 100%.

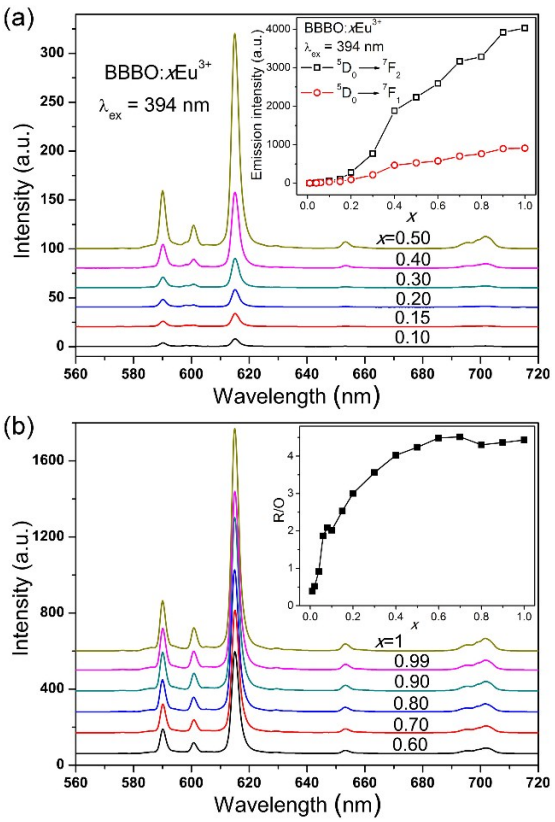

Fig. 8 Emission spectra of **BBBO:xEu^{3+}** ($0 \le x \le 1$) under 394 nm excitation. The inserts show the respective intensities of $^5D_0 \rightarrow {}^7F_1$ and $^5D_0 \rightarrow {}^7F_2$ emissions, and the R/O values against the dopant concentration.

Moreover, as shown in Fig. 3, the intensities of the *f-f* excitation peaks of Eu^{3+} also increase along with x, which proposes that Eu^{3+}-doped **BBBO** can also be efficiently excited by UV-LED chips. Fig. 8 gives the emission spectra of **BBBO:xEu^{3+}** samples under the excitation of 394 nm. The variations of the emission intensities and the R/O values with Eu^{3+} concentration are also given in the inserts. Both of the intensities of $^5D_0 \rightarrow {}^7F_1$ and $^5D_0 \rightarrow {}^7F_2$ transitions increase with x, and no quenching or saturation effect was observed. The

variation tendency of R/O is similar with that excited by Bi^{3+} absorption, which increases with the Eu^{3+} concentration first, and saturated when $x \geq 0.60$. The R/O values are generally larger than those excited by Bi^{3+} absorption especially for those low Eu^{3+} content samples. The bright emission under 394 nm excitation and large R/O values (~4.5 when $x \geq 0.70$) imply this series of samples may also be good candidates for red-emitting UV-LED phosphors.

Table 1 Quantum yields (QYs) of **BBBO:*x*Eu^{3+}**, $Ba_6(La_{0.2}Bi_{0.1}Eu_{0.7})_9B_{79}O_{138}$ under 269 nm excitation, and commercial Y_2O_3:Eu^{3+} under 254 nm excitation, respectively.

x in ***BBBO:xEu^{3+}***	*Quantum yields (%)*
0.10	33
0.20	33
0.50	62
0.70	86
0.80	72
$Ba_6(La_{0.2}Bi_{0.1}Eu_{0.7})_9B_{79}O_{138}$	98
Commercial Y_2O_3:Eu^{3+}	~100

Comparing to the inert nature of Eu^{3+} *f-f* absorptions, the position of the $^1S_0 \rightarrow {}^3P_1$ transition of Bi^{3+} is sensitive to the surrounding environment. The coexistence of Bi^{3+}-to-Eu^{3+} energy transfer and the symmetry change of local coordination complicate the changing tendency of the Bi^{3+} absorption, both in intensity and position (see Figs. 3 and 4). For instance, as shown in Fig. 4, the shifting of the peak wavelength of Bi^{3+} absorption along with *x* can be divided into three region, *x* = 0.01-0.30, 0.30-0.70, and 0.70-0.99. Indeed, the local symmetry of Eu^{3+} maintains as centrosymmetric and noncentrosymmetric in the region of *x* = 0.01-0.30 and 0.70-0.99, respectively; in the middle region of *x* = 0.30-0.70, a gradual symmetry change occurs. Therefore, the two blue shifting of the excitation wavelength of Bi^{3+} with *x* in the regions of *x* = 0.01-0.30 and 0.70-0.99 are perhaps due to the replacement of Bi^{3+} by Eu^{3+} with smaller ionic radii. Similar phenomenon has been found in Bi^{3+} and Tb^{3+} co-doped $GdAlO_3$, in which the excitation wavelength of Bi^{3+} showed a linear shifting when Gd^{3+} ions were replaced by Bi^{3+} with larger ionic radii.[27] While, the red shifting in the middle region of *x* = 0.30-0.70 originates from the local symmetry change from centrosymmetric to noncentrosymmetric.

Sensitization effect of Bi^{3+} to Eu^{3+} in $Ba_6(La_{0.3-y}Bi_yEu_{0.7})_9B_{79}O_{138}$ ($0 \leq y \leq 0.3$)

Here, the direct energy transfer from Bi^{3+} to Eu^{3+} was observed in **BBBO:*x*Eu^{3+}** system. In order to confirm the energy transfer mode and investigate the sensitization effect of Bi^{3+} to Eu^{3+}, we fixed the concentration of Eu^{3+} at 0.7 and replaced Bi^{3+} by La^{3+} in the solid solutions $Ba_6(La_{0.3-y}Bi_yEu_{0.7})_9B_{79}O_{138}$ ($0 \leq y \leq 0.3$). A relatively high doping level of Eu^{3+} is benefit for obtaining bright red emission and the local structure is sustained in this region according to the above analysis. Fig. 9a shows the excitation spectra of $Ba_6(La_{0.3-y}Bi_yEu_{0.7})_9B_{79}O_{138}$ by monitoring the Eu^{3+} emission wavelength of 615 nm. The broad band centering at 246 nm in the excitation spectrum of $Ba_6(La_{0.3}Eu_{0.7})_9B_{79}O_{138}$ is the typical $O^{2-} \rightarrow Eu^{3+}$ CT transition, and the broad bands with the maximum at 267 nm in other three spectra are the $^1S_0 \rightarrow {}^3P_1$ transition of Bi^{3+}. The presence of intense Bi^{3+} absorption indicates there is a strong energy transfer from Bi^{3+} to Eu^{3+}. The emission spectra of these samples (see Fig. 9b) do not contain any emission form Bi^{3+}, further consolidating the effective energy transfer.

The insert in Fig. 9b gives the calculated emission intensities of $Ba_6(La_{0.3-y}Bi_yEu_{0.7})_9B_{79}O_{138}$ ($0 \leq y \leq 0.3$) samples and digital photographs under a 254 nm UV lamp excitation. Comparing to the Bi^{3+}-free sample, it is quite interesting that the intensity of Eu^{3+} emission was almost doubled by introduce of only 10 atom% Bi^{3+}. Apparently, $Ba_6(La_{0.2}Bi_{0.1}Eu_{0.7})_9B_{79}O_{138}$ show a higher PL intensity than two end members, $Ba_6(La_{0.3}Eu_{0.7})_9B_{79}O_{138}$ and $Ba_6(Bi_{0.3}Eu_{0.7})_9B_{79}O_{138}$. The QY of $Ba_6(La_{0.2}Bi_{0.1}Eu_{0.7})_9B_{79}O_{138}$ under 269 nm excitation is 98%, as shown in Table 1, which is very close to the commercial Y_2O_3:Eu^{3+} red phosphor under 254 nm excitation.

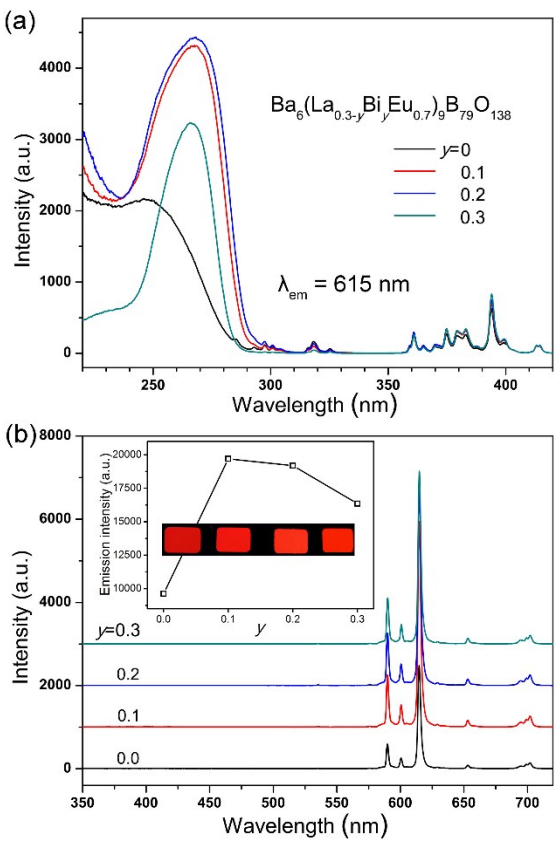

Fig. 9 (a) Excitation and (b) emission spectra of the $Ba_6(La_{0.3-y}Bi_yEu_{0.7})_9B_{79}O_{138}$ ($0 \leq y \leq 0.3$, λ_{em} = 615 nm, λ_{ex} = 267 nm). The insert gives the variation of the calculated emission intensities along with Bi^{3+} concentration (*y*) and the digital photographs under a 254 nm UV lamp excitation.

Conclusions

Solid solutions of $Ba_6(Bi_{1-x}Eu_x)_9B_{79}O_{138}$ ($0 \leq x \leq 1$) and $Ba_6(La_{0.3-y}Bi_yEu_{0.7})_9B_{79}O_{138}$ ($0 \leq y \leq 0.3$) were synthesized by

high temperature solid-state reaction, whose photoluminescence properties were systematically studied. Our anticipation of the highly efficient Bi^{3+}-to-Eu^{3+} energy transfer was confirmed, which indeed led to bright and pure-red phosphors by suitable Eu^{3+}-doping into **BBBO**. In fact, the Eu^{3+}-doping introduced a site-symmetry evolution from centrosymmetric in low-level substitutions ($x < 0.3$) to noncentrosymmetric when $x > 0.7$. When x is between 0.3 and 0.7, a continuous changing occurs which caused a red-shifting of the wavelength of Bi^{3+} absorption accompanied by a sharp increase of R/O ratios of Eu^{3+} emission. Such a three-region-characteristic was attributed to the site symmetry changing of the Bi^{3+}/Eu^{3+} coordination, leading to a synergetic effect on the evolution of Bi^{3+} $^1S_0 \rightarrow {}^3P_1$ absorption and R/O ratios. Moreover, we found that slight reducing the Bi^{3+} concentration by La^{3+}-substitution could further enhance the emission intensity and QY, for example, $Ba_6(La_{0.2}Bi_{0.1}Eu_{0.7})_9B_{79}O_{138}$ shows a higher PL intensity and QY value (98%) than $Ba_6(Bi_{0.3}Eu_{0.7})_9B_{79}O_{138}$ (86%). **BBBO** is a new polyborate host with a freshly resolved and complex structure, the current preliminary and interesting results promote us to further develop **BBBO**-based phosphors.

Acknowledgements

This work was financially supported by the Nature Science Foundation of China (grants 21101175, 21171178, 91222106) and Natural Science Foundation Project of Chongqing (grants 2012jjA0438, 2014jcyjA50036). The Fundamental Research Funds for the Central Universities (grant CQDXWL-2014-005) also partially supported this work.

Notes and references

[a] College of Chemistry and Chemical Engineering, Chongqing University, Chongqing 400044, People's Republic of China. Email: congrihong@cqu.edu.cn, taoyang@cqu.edu.cn; Tel: +86-23-65105065.
[b] School of Science, Chongqing University of Posts and Telecommunications, Chongqing 400065, People's Republic of China.

Electronic Supplementary Information (ESI) available: unit cell parameters of $Ba_6(La_{0.3-y}Bi_yEu_{0.7})_9B_{79}O_{138}$ ($0 \le y \le 0.3$), structural figures of Bi^{3+} coordination in BBBO. See DOI: 10.1039/b000000x/

1. D. Y. Wang, T. M. Chen, B. M. Cheng, *Inorg. Chem.*, 2012, **51**, 2961-2965.
2. A. Szczeszak, T. Grzyb, B. Barszcz, V. Nagirnyi, A. Kotlov, S. Lis, *Inorg. Chem.*, 2013, **52**, 4934-4940.
3. N. Pradal, D. Boyer, G. Chadeyron, S. Therias, A. Chapel, C. V. Santilli, R. Mahiou, *J. Mater. Chem. C*, 2014, **2**, 6301-6311.
4. Z. Yang, J. H. Lin, M. Z. Su, *Acta Chem. Sin.*, 2001, **59**, 736-741.
5. M. He, G. L. Huang, H. L. Tao, Z. H. Zhang, *Physica B*, 2012, **407**, 2725-2728.
6. X. F. Yi, R. H. Cong, Z. Y. Zhou, P. F. Jiang, W. L. Gao, T. Yang, *New J. Chem.*, 2014, **38**, 122-131.
7. X. R. Sun, W. L. Gao, T. Yang, R. H. Cong, *Dalton Trans.*, 2015, **44**, 2276-2284.
8. S. Saubat, M. Vlasse, C. Fouassier, *J. Solid State Chem.*, 1980, **34**, 271-277.
9. W. T. Fu, C. Fouassier, P. Hagenmuller, *Mater. Res. Bull.*, 1987, **22**, 389-397.
10. W. T. Fu, C. Fouassier, P. Hagenmuller, *Mater. Res. Bull.*, 1987, **22**, 899-909.
11. Z. Yang, J. H. Lin, M. Z. Su, L. P. You, *Mater. Res. Bull.*, 2000, **35**, 2173-2182.
12. R. P. Sonekar, S. K. Omanwar, S. V. Moharil, P. L. Muthal, S. M. Dhopte, V. K. Kondawar, *J. Lumin.*, 2009, **129**, 624-628.
13. W. Park, C. J. Summers, Y. R. Do, H. G. Yang, *J. Mater. Sci.*, 2002, **37**, 4041-4045.
14. J. T. Ingle, R. P. Sonekar, S. K. Omanwar, Y. H. Wang, L. Zhao, *J. Alloys Compd.*, 2014, **608**, 235-240.
15. Z. Yang, J. H. Lin, M. Z. Su, Y. Tao, W. Wang, *J. Alloys Compd.*, 2000, **308**, 94-97.
16. A. M. Srivastava, M. T. Sobieraj, R. Gieger, E. Banks, *Mater. Chem. Phys.*, 1989, **21**, 327-333.
17. Z. Yang, J. H. Lin, M. Z. Su, *Sci. China Ser. B*, 2001, **44**, 1-6.
18. H. J. Zhang, Y. H. Wang, L. L. Han, *J. Appl. Phys.*, 2011, **109**, 053109.
19. Y. L. Huang, H. Lin, H. J. Seo, *J. Electrochem. Soc.*, 2010, **157**, J405-J409.
20. H. Lin, Y. L. Huang, H. Seo, *J. Phys. Status Solidi A*, 2010, **207**, 1210-1215.
21. X. Z. Li, X. L. Chen, J. K. Lian, L. Wu, Y. P. Xu, Y. G. Cao, *J. Alloys Compd.*, 2004, **365**, 277-280.
22. H. P. You, X. Y. Wu, X. Q. Zeng, G. Y. Hong, C. H. Kim, C. H. Pyun, C. H. Park, *Mater. Sci. Eng. B*, 2001, **86**, 11-14.
23. Y. Ji, J. Liang, S. Xie, X. Wu, *J. Cryst. Growth*, 1994, **137**, 521-527.
24. C. F. Shen, L. L. Ximen, X. F. Zong, *Mater. Res. Bull.*, 1989, **24**, 1223-1230.
25. R. H. Cong, Z. Y. Zhou, Q. Q. Li, J. L. Sun, J. H. Lin, T. Yang, *J. Mater. Chem. C*, 2015, **3**, 4434-4437.
26. X. T. Wei, Y. H. Chen, X. R. Cheng, M. Yin, W. Xu, *Appl. Phys. B*, 2010, **99**, 763-768.
27. J. Y. Park, H. C. Jung, G. S. R. Raju, B. K. Moon, J. H. Jeong, S. M. Son, J. H. Kim, *Mater. Res. Bull.*, 2010, **45**, 572-575.
28. *TOPAS, V4.1-beta*, Bruker AXS, Karlsruhe, Germany, 2004.
29. B. S. Naidu, B. Vishwanadh, V. Sudarsan, R. K. Vatsa, *Dalton Trans.*, 2012, **41**, 3194-3203.
30. L. Chen, H. Zheng, J. Cheng, P. Song, G. Yang, G. Zhang, C. Wu, *J. Lumin.*, 2008, **128**, 2027-2030.
31. H. S. Yoo, W. Bin Im, J. H. Kang, D. Y. Jeon, *Opt. Mater.*, 2008, **31**, 131-135.

Graphic Abstract

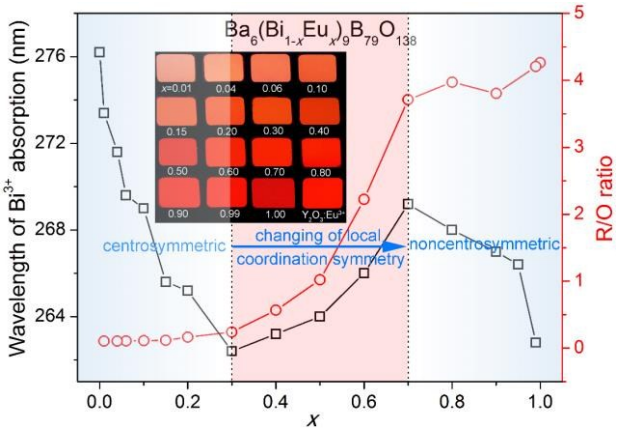

$Ba_6(Bi_{1-x}Eu_x)_9B_{79}O_{138}$:$xEu^{3+}$ shows a simultaneous changing in the wavelength shifting of Bi^{3+} absorption and the red-to-orange emission ratio by varying *x*.